Article

Statistical Interdependence between Daily Precipitation and Extreme Daily Temperature in Regions of Mexico and Colombia

Álvaro Zabaleta-Ortega [1], Teobaldis Mercado-Fernández [2], Israel Reyes-Ramírez [1], Fernando Angulo-Brown [3] and Lev Guzmán-Vargas [1,*]

1   Unidad Profesional Interdisciplinaria en Ingeniería y Tecnologías Avanzadas, Instituto Politécnico Nacional, Ciudad de México 07340, Mexico; azabaletao1900@alumno.ipn.mx (Á.Z.-O.); ireyesr@ipn.mx (I.R.-R.)
2   Facultad de Ciencias Agrícolas, Universidad de Córdoba, Cra. 6 #77-305, Montería 230002, Colombia; tmercado@correo.unicordoba.edu.co
3   Departamento de Física, Escuela Superior de Física y Matemáticas, Instituto Politécnico Nacional, Ciudad de México 07738, Mexico; angulo@esfm.ipn.mx
*   Correspondence: lguzmanv@ipn.mx; Tel.: +52-(55)57-29-6000 (ext. 56873)

Abstract: We study the statistical interdependence between daily precipitation and daily extreme temperature for regions of Mexico (14 climatic stations, period 1960–2020) and Colombia (7 climatic stations, period 1973–2020) using linear (cross-correlation and coherence) and nonlinear (global phase synchronization index, mutual information, and cross-sample entropy) synchronization metrics. The information shared between these variables is relevant and exhibits changes when comparing regions with different climatic conditions. We show that precipitation and temperature records from La Mojana are characterized by high persistence, while data from Mexico City exhibit lower persistence (less memory). We find that the information exchange and the level of coupling between the precipitation and temperature are higher for the case of the La Mojana region (Colombia) compared to Mexico City (Mexico), revealing that regions where seasonal changes are almost null and with low temperature gradients (less local variability) tend to display higher synchrony compared to regions where seasonal changes are very pronounced. The interdependence characterization between precipitation and temperature represents a robust option to characterize and analyze the collective dynamics of the system, applicable in climate change studies, as well as in changes not easily identifiable in future scenarios.

Keywords: time series; precipitation; temperature; entropy; synchronization

1. Introduction

Statistical interdependency can quantify interactions between systems' elements when they evolve synchronously [1–3]. It focuses on assertively quantifying the coupling responsible for collective behavior. One of the most fruitful approaches to understand this phenomenon is Kuramoto's pioneering study in the 1970s on the phase synchronization analysis of coupled oscillators [4]. A number of studies have applied these notions to synchronization analysis between irregular signals, identifying different coupling levels in several fields, including physical and biological systems [5–7]. However, despite its usefulness in studying different systems [8], the complex nature of systems has given rise to mathematical complications in this task [9].

From a practical point of view, the evaluation of the coupling level between complex signals requires the incorporation of different approaches. A group of methods which have proved to be very useful in measuring coupling between irregular signals are those derived from information theory or that are entropy based, whose principal applications have focused on physiological signal analysis [10–27] but are also applied in other fields such as finance [28–31], Earth sciences [32–34], and engineering [35], among others.

On the other hand, climate is a complex system whose behavior requires an integrated approach to describe its dynamics [36,37] and especially the characterization of coupling levels between representative variables. In past years, a great variety of coupling measures have been applied in the context of the climate study. For instance, Duane [38] studied meteorological teleconnections, using synchronized chaos, and reported the tendency of two hemispheric subsystems that simultaneously occupy the same regime. Berg et al. [39] analyzed seasonal characteristics of the relationship between daily precipitation intensity and surface temperature in Europe, distinguishing separate precipitation types and stating the dependence between temperature and precipitation. Donges et al. [40] compared measures to analyze climatic teleconnections using a complex network approach. Feliks et al. [41] studied the synchronization between the North Atlantic Oscillation and Oscillatory Climate Modes in the Eastern Mediterranean, identifying a significant synchronization. On the other hand, Gennaretti et al. [42] used the correlation coefficient to evaluate the interdependence of average temperature and precipitation for Canadian Arctic coastal zones, highlighting the importance of including interdependence analysis on climate change scenarios, and Jajcay et al. [43] analyzed the causality and synchronization of the El Niño Southern Oscillation, ENSO, and stated that the understanding of founded discrepancies may be the key to improving the ENSO prediction.

Two of the most important and representative climatic variables are precipitation and temperature because they play a key role in the hydrological behavior of a territory with an impact on events such as floods and droughts, among others [44–46]. These variables (as physical phenomena) exchange nontrivial information in their (joint) evolution and are indispensable in the climate characterization. Quantifying the coupling level between climatic variables such as precipitation and temperature represents valuable information to robustly characterize their collective behavior, which is relevant in studies of climate change scenarios. However, as mentioned above, the description and characterization of climate variables have mainly focused on analyzing teleconnections and seasonal relationships. Nonetheless, there is a gap in the interdependence study to quantify shared information between climate variables such as precipitation and daily extreme temperature using robust techniques of synchronization measures, which is covered in this paper. In this work, the interdependence between precipitation and extreme daily temperature (maximum and minimum) is studied by measuring their synchronization level. We start with a statistical description of the time series by exploratory data analysis. The initial approach to the synchronization is studied using the cross-correlation and coherence functions, whereas the deeper analysis is carried out using the mutual information, the global phase synchronization index and the cross-sample entropy.

The remainder of this paper is outlined as follows: Section 2 contains the material and methods, which describe the study area, data, and data treatment for applying the techniques of synchronization measures. Section 3 presents the results and discussions of the obtained values from the applied techniques and their dissertation. Finally, Section 4 includes the conclusions.

2. Materials and Methods

2.1. Study Area and Data

We studied climatic data from two regions. The first one is the metropolitan area of Mexico City (Mexico), one of the most populated cities in the world, where urban expansion has introduced modifications in the atmospheric energy exchange [47]. Daily records of precipitation, and maximum and minimum temperatures of 14 climatic stations from 1960 to 2020 were studied, i.e., 42 time series each with about 20,000 records obtained from Servicio Meteorológico Nacional (SMN) of the Comisión Nacional del Agua (CONAGUA, https://smn.conagua.gob.mx/es/climatologia/informacion-climatologica/informacion-estadistica-climatologica, last accessed date: 8 May 2024). The second region refers to La Mojana (Colombia), which serves as a hydraulic damping system for the Cauca, San Jorge, and Brazo Loba (a bifurcation of Magdalena River) rivers that convert it in a

great interest area due to its natural diversity, hydrological and hydraulic functions, and agricultural importance with particular climate characteristics and social dynamic [48,49]. For this region, the precipitation and maximum temperature daily records of seven (07) climatic stations between 1973 and 2020 were studied, i.e., 14 time series of about 13,500 records each, obtained upon request to the Instituto de Hidrología, Meteorología y Estudios Ambientales (IDEAM, http://dhime.ideam.gov.co/atencionciudadano/, last accessed date: 8 May 2024). In total, 56 time series were studied. The records period for each region was taken according to the data availability. Because of the information's lack of minimum temperature, it was not possible to study this variable for La Mojana. The general relevant information on climatic stations is shown in Table 1. To visualize the study area, see detailed online information on the geographical location of the stations at this link: https://colab. research.google.com/drive/1ZWVi9hpvi_Q3ZeR4BOhgTat3sR7l_kbN?usp=sharing, last accessed date: 8 May 2024.

Table 1. General information of climatic stations.

Station	Station Code	Latitude	Longitude	Altitude (msnm)
Mexico City				
MCS1	9010	19.4125	−99.2017	2271
MCS2	9014	19.3033	−99.1481	2256
MCS3	9071	19.3339	−99.1322	2250
MCS4	9020	19.2969	−99.1822	2296
MCS5	9029	19.4767	−99.0914	2239
MCS6	9022	19.1344	−99.1731	2990
MCS7	9032	19.1906	−99.0219	2420
MCS8	9036	19.3953	−99.0978	2235
MCS9	9068	19.4292	−99.0528	2240
MCS10	9041	19.1967	−99.1286	2620
MCS11	9043	19.4653	−99.0792	2620
MCS12	9045	19.1789	−99.0028	2240
MCS13	9048	19.4036	−99.1961	2595
MCS14	9051	19.2628	−99.0036	2309
La Mojana				
LMS1	25025100	9.28194	−74.84528	18
LMS2	25025150	8.29519	−75.16450	20
LMS3	25015010	8.18078	−75.63228	170
LMS4	25025170	8.74086	−75.49883	125
LMS5	25025240	8.54283	−74.63556	20
LMS6	25025210	8.92075	−74.47425	10
LMS7	25025190	8.39933	−75.58372	90

2.2. Exploratory and Fractal Data Analysis

This aspect was addressed through descriptive statistics, involving position and central tendency measures and dispersion measures, among other statistics measures, following [50–53]. The missing data were input using reanalysis data obtained from ERA database (https://cds.climate.copernicus.eu/cdsapp#!/dataset/reanalysis-era5-single-levels? tab=form, last accessed date: 8 May 2024). Also, through visual inspection, we identified outliers, and if any existed, we compared them with nearby stations searching for similar records at the occurrence date. If such an event was an extreme one, we validated it, and we replaced it with the ERA register otherwise. In addition, to characterize the temporal organization of the individual (univariate) series, persistence and fractality were analyzed using rescaled range analysis [54] and Higuchi's fractal dimension [55]. Details of the procedures for calculating the Hurst exponent (H) and the Higuchi fractal dimension (D) can be found in [56] and [55,57], respectively. Values of $0.5 < H \leq 1.0$ indicate persistence

(long-term memory), while $0.0 \leq H < 0.5$ indicates anti-persistence, and if $H = 0.5$, the fluctuations are neither persistent nor anti-persistent. Similarly, signals with $D < 1.5$ exhibit long-range correlations, while $D > 1.5$ indicates anti-correlations. There is a direct relationship between H and D that is applicable to self-affine series given by $H = 2 - D$, where $1 < D < 2$ [58].

2.3. Synchronization Measures

Let P, T_{max}, and T_{min} be the precipitation, and maximum and minimum temperatures, respectively. We compute the following measures.

2.3.1. Cross-Correlation Function

The *cross-correlation function* $c_{P,T}(\tau)$ between P and T (T_{max} or T_{min} as appropriate) gives a linear synchronization measure between P and T at a lag τ, expressed as [59,60]:

$$c_{P,T}(\tau) = \frac{1}{N - \tau} \sum_{i=1}^{N-\tau} \frac{(P_i - \bar{P})(T_{i+\tau} - \bar{T})}{s_P s_T}, \tag{1}$$

where N is the time series size, and $\bar{P}$ and $\bar{T}$ represent the mean values. s_P and s_T denote the standard deviation of P and T, respectively.

2.3.2. Coherence Function

The *coherence function* $\Gamma_{P,T}(f)$ gives a linear synchronization measure in the frequency domain, involving the Fourier transform of the cross-correlation function of P and T, modulated with its self-spectral [61,62], that is:

$$\Gamma_{P,T}(f) = \frac{G_{P,T}(f)}{\sqrt{G_{P,P}(f) G_{T,T}(f)}}, \tag{2}$$

where $G_{P,T}(f) = \int_{-\infty}^{\infty} c_{P,T}(\tau) e^{j2\pi f\tau} d\tau$ is the crossed spectral of P and T, and $c_{P,T}(\tau)$ is the mathematical expectation cross-correlation function. $G_{P,P}(f)$ and $G_{T,T}(f)$ are the self-spectrals of the mathematical expectation of the autocorrelation function of P and T, respectively.

2.3.3. Mutual Information

Mutual information $MI(P,T)$ is an entropy-based measure that quantifies the information amount shared between the random variables P and T with marginal distributions $p(P)$, $p(T)$ and joint distribution $p(P,T)$ computed as [63–65]:

$$MI(P,T) = \sum_{x \in P} \sum_{y \in T} p(x,y) \log \frac{p(x,y)}{p(x)p(y)}, \tag{3}$$

The $MI(P,T)$ also gives a stable measure of the information flow of the variables in terms of its synchronization.

2.3.4. Global-Phase Synchronization Index Using Hilbert Transform

This measure is based on analyzing the instantaneous phases $\Delta\phi_{P,T}(t)$ of the signals P and T, whose remarkable characteristics are the signal phase analysis, irrespective of their frequency and nonparametric condition, and are defined as [5,15,24,62]:

$$\gamma_{P,T}(t) = \sqrt{\langle \cos(\Delta\phi_{P,T}(t)) \rangle^2 + \langle \sin(\Delta\phi_{P,T}(t)) \rangle^2},$$

$$\Delta\phi_{P,T}(t) = \arctan\left[\frac{\tilde{S}_P(t)S_T(t) - \tilde{S}_T(t)S_P(t)}{S_P(t)S_T(t) + \tilde{S}_P(t)\tilde{S}_T(t)}\right], \tag{4}$$

$$\tilde{S}.(t) = \mathcal{H}(P(t)) = PV\frac{1}{\pi}\int_{-\infty}^{\infty}\frac{S.(t)}{t - \tau}d\tau,$$

where $\tilde{S}.(t)$ is the Hilbert transform of the signal ($P(t)$ or $T(t)$ as appropriate), and PV is Cauchy's principal value.

2.3.5. Cross-Sample Entropy

Cross − sample entropy, here denoted as CSE, is an entropy-based asynchrony measurement that compares the similarity between two time series. CSE depends on three parameters: m is the model vector's length, r is the distance tolerance, and N is the time series size. To compute CSE, we proceed as follows [13,14,17]: given the time series (signals) $u(t) = P(1), P(2), \cdots, P(N)$ and $v(t) = T(1), T(2), \cdots, T(N)$ (just P, T_{max} or T_{min} as appropriate), we compute $B^m(r)(P||T) = \frac{1}{N-m}\sum_{i=1}^{N-m} B_i^m(r)(P||T)$, where $B_i^m(r)(P||T) = \frac{1}{N-m-1}\sum_{i,j=1;i\neq j}^{N-m} \Theta(r - ||u_i^m - v_j^m||)$, $\Theta(\cdot)$ is the Heaviside step function, $||u_i^m - v_j^m||$ is the Euclidean distance between $u_i^m = P(i), P(i+1), \cdots, P(i+m-1)$ and $v_j^m = T(j), T(j+1), \cdots, T(j+m-1)$; $1 \leq i,j \leq N-m-1$. Similarly, we calculate $A^m(r)(P||T) = \frac{1}{N-m}\sum_{i=1}^{N-m} A_i^m(r)(P||T)$, where $A_i^m(r)(P||T) = \frac{1}{N-m-1}\sum_{i,j=1;i\neq j}^{N-m} \Theta(r - ||u_i^{m+1} - v_j^{m+1}||)$. Finally, the CSE is defined as:

$$CSE(m, r, N) = -\ln\left(\frac{A^m(r)(P||T)}{B^m(r)(P||T)}\right). \tag{5}$$

CSE is zero when the time series are perfectly synchronized, whereas higher values of CSE indicate asynchrony.

2.4. Statistical Significance Test for the Synchronization Metrics

To investigate differences in the metrics obtained between the two regions, using the `Scipy stats` module (https://docs.scipy.org/doc/scipy/reference/stats.html, last accessed date: 8 May 2024), we computed the *t*-Student test, which is a statistic test that, with a defined significance level (or its equivalent confidence level), compares if two independent samples are similar regarding their mean values [66], and the Mann–Whitney test [67], a nonparametric statistic test that compares if two independent variables are dissimilar.

The set of coupling measures described above allows us to quantify the synchronization degree between precipitation and temperature covering both linear (cross-correlation and coherency function) and nonlinear (mutual information, phase synchronization, and cross-sample entropy) information aspects by studying them in the time (cross-correlation function and entropy-based measures), frequency (coherence function), and phase (phase synchronization index) domains. These metrics provide us with valuable information on the joint evolution to characterize and analyze the relationship between these climatic variables further than conventional statistical analysis. All data processing and metrics computations were carried out in `Python` (https://www.python.org/, last accessed date: 8 May 2024) language, using libraries such as `Numpy` (https://numpy.org/, last accessed date: 8 May 2024), `Scipy` (https://scipy.org/, last accessed date: 8 May 2024), `EntropyHub` (https://www.entropyhub.xyz/, last accessed date: 8 May 2024) and `Matplotlib` (https://matplotlib.org/, last accessed date: 8 May 2024) for graphical visualization. The results are described below.

3. Results and Discussion

3.1. Exploratory Data Analysis

Figure 1 illustrates representative time series under analysis for both regions. For the analyzed period in Mexico City (1960–2020), the maximum temperature recorded values between 3.5 °C and 38.5 °C, with a mean value of 23.3 °C, the minimum temperature registered values ranging from −10.5 °C to 26.0 °C with a mean value of 8.3 °C, while the precipitation presented the maximum value of 117 mm in 24 h. The maximum temperature exhibits dispersion below the first quartile and above the third quartile, showing higher

variability in the extremes. On the other hand, the minimum temperature shows less variability in the extreme values. In La Mojana, for the analyzed period (1973–2020), the maximum temperature ranges from 22.6 °C to 46.9 °C, whose mean value oscillates around 31.6 °C. The highest precipitation event reported has a magnitude of 301.3 mm. In general, the maximum temperature in the Mojana is less dispersed than in Mexico City, with a concentration between the first and third quartiles. Figure 2 shows the boxplot of the analyzed climatic variables.
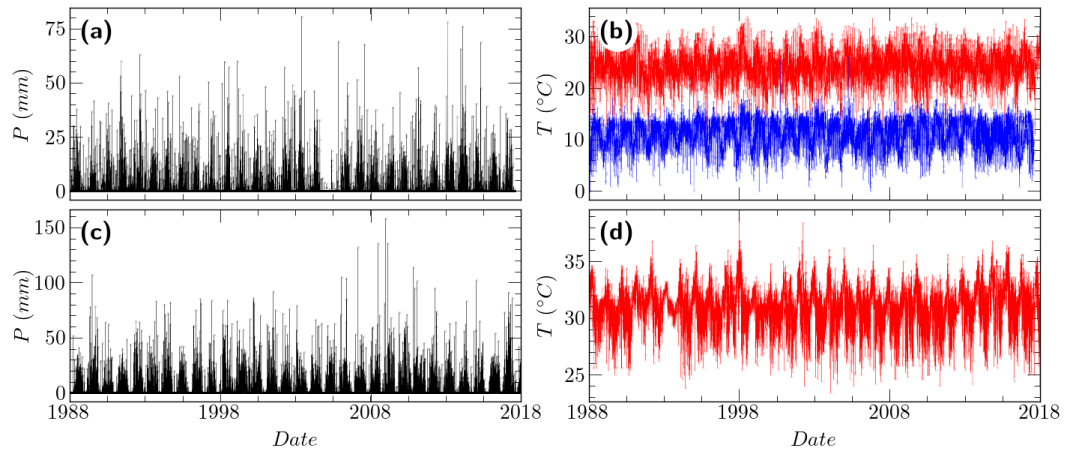

Figure 1. Representative time series of (**a**) precipitation P and (**b**) maximum and minimum temperatures T (T_{max}, red line; T_{min}, blue line, respectively) for Mexico City (station MCS13). (**c**) Precipitation P and (**d**) maximum temperature T (T_{max}) for La Mojana (station LMS4).

The data structure was studied through its persistence and fractality. The persistence was analyzed using Hurst exponent H obtained with the rescaled range method, which indicates the presence of long-term correlations among the records. For all variables under study and both regions, Mexico City and La Mojana, Hurst values fall within the interval $0.5 < H \le 1.0$ (see Table 2). For precipitation, the magnitude of certain rainfall events has a long-term relationship, and the same applies for the temperature as well. For Mexico City, it is observed that $H_{T_{min}} > H_{T_{max}} > H_P$ and for La Mojana, $H_{T_{max}} > H_P$. These results indicate that these climatic variables have different levels of long-term correlations, i.e., "process memory". Moreover, these results agree with other studies in terms of the persistence values for the scaling indexes in different climate analysis [56,68–75].

Table 2. Hurst exponent values H for P (H_P), T_{max} ($H_{T_{max}}$) and T_{min} ($H_{T_{min}}$).

Mexico City							
Station	H_P	$H_{T_{max}}$	$H_{T_{min}}$	**Station**	H_P	$H_{T_{max}}$	$H_{T_{min}}$
MCS1	0.78	0.83	0.85	MCS8	0.78	0.83	0.85
MCS2	0.78	0.83	0.85	MCS9	0.78	0.83	0.85
MCS3	0.78	0.83	0.85	MCS10	0.78	0.83	0.84
MCS4	0.81	0.83	0.84	MCS11	0.78	0.83	0.84
MCS5	0.77	0.83	0.84	MCS12	0.78	0.83	0.85
MCS6	0.78	0.83	0.82	MCS13	0.77	0.77	0.83
MCS7	0.84	0.83	0.83	MCS14	0.78	0.83	0.84
La Mojana							
Station	H_P	$H_{T_{max}}$		**Station**	H_P	$H_{T_{max}}$	
LMS1	0.83	0.87		LMS5	0.75	0.78	
LMS2	0.76	0.82		LMS6	0.77	0.79	
LMS3	0.77	0.84		LMS7	0.77	0.81	
LMS4	0.74	0.86		—	—	—	
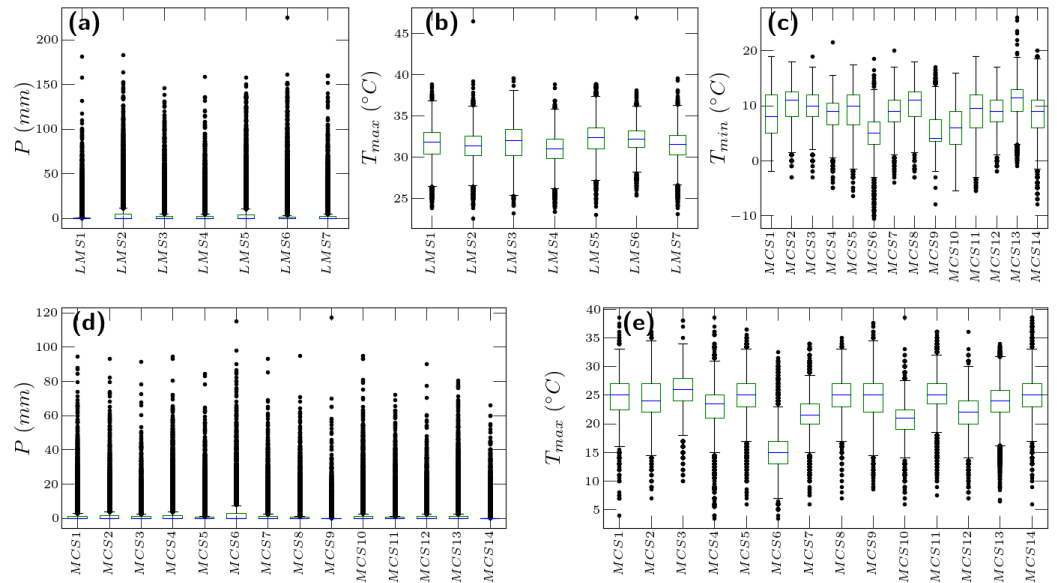
Figure 2. Boxplot of raw data. (**a**,**b**) correspond to the precipitation and maximum temperature, respectively, for La Mojana. (**c**–**e**) correspond to the minimum temperature, precipitation and maximum temperature for Mexico City, respectively. In general, the temperature exhibits more dispersion in Mexico City than in La Mojana, whereas for precipitation, it shows a similar behavior. In all variables, higher event values are observed for La Mojana, which shows important differences in the fluctuations between the two climatic regions.

On the other hand, Table 3 shows the results of the Higuchi fractal dimension (D). We find that, in general, $D_P > D_{T_{max}} > D_{T_{min}}$, preserving the same hierarchy in the irregularity of the structure in the variables from both regions. When the fractal dimension associated with precipitation is compared between regions, we observe that, in most cases, the one corresponding to Mexico City is larger than the one corresponding to La Mojana, confirming that there is a greater irregularity in the former. Thus, precipitation tends to be a very irregular phenomenon and therefore difficult to predict, while the relative regularity of temperature makes it somewhat more predictable. In addition, the results shown in Table 3 are consistent with the long-term self-correlations presented in Table 2 for the Hurst exponent, and the values satisfy the known $H = 2 - D$ relationship.

Table 3. Higuchi fractal dimension D values for P, T_{max} and T_{min}.

Mexico City							
Station	D_P	$D_{T_{max}}$	$D_{T_{min}}$	**Station**	D_P	$D_{T_{max}}$	$D_{T_{min}}$
MCS1	1.26	1.21	1.15	MCS8	1.28	1.21	1.15
MCS2	1.26	1.23	1.15	MCS9	1.25	1.21	1.14
MCS3	1.25	1.22	1.14	MCS10	1.27	1.21	1.16
MCS4	1.25	1.22	1.16	MCS11	1.31	1.23	1.15
MCS5	1.30	1.23	1.15	MCS12	1.25	1.23	1.15
MCS6	1.23	1.23	1.27	MCS13	1.28	1.23	1.17
MCS7	1.27	1.23	1.16	MCS14	1.29	1.22	1.14
La Mojana							
Station	D_P	$D_{T_{max}}$		**Station**	D_P	$D_{T_{max}}$	
LMS1	1.22	1.13		LMS5	1.21	1.15	
LMS2	1.19	1.15		LMS6	1.24	1.16	
LMS3	1.24	1.17		LMS7	1.23	1.17	
LMS4	1.25	1.14		——	——	——	——

As a general approach of linear correspondence, the global Pearson correlation (which, roughly speaking, is a linear correspondence relationship between two independent variables) between the precipitation and temperature (maximum T_{max} and minimum T_{min} as appropriate) is computed for all the variables for each region (Mexico City an La Mojana), and the results are illustrated in Figure 3. It can be seen from the correlation matrix in Figure 3 that there is a high global relationship between the variables as the climatic zone correspondence.

In general, according to Figure 3, La Mojana exhibits higher values of Pearson correlations than Mexico City. This effect is possibly due to the higher relative stability of climatic variables in La Mojana, which has a stretched interval of occurrence values compared with those from Mexico City.
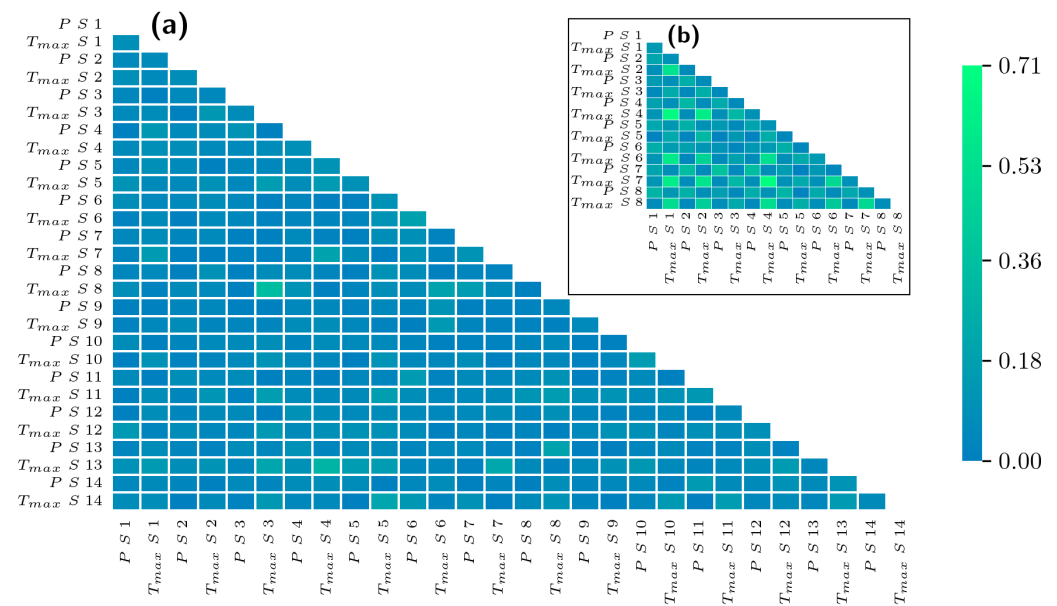
Figure 3. Global Pearson correlation coefficient matrix between precipitation and maximum temperature of empirical data in (**a**) Mexico City and (**b**) La Mojana.

3.2. Synchronization Measures

To reduce the effects of spurious correlations that can affect the applied techniques and lead to misleading results, we normalized the time series before computing the synchronization measures by extracting its mean and dividing by the standard deviation such that the time series are normalized to have zero mean and unitary variance.

3.2.1. Cross-Correlation Function

After exploring the Pearson correlation comparing all the variables between them for each regions, we evaluated the linear synchronization as time dependence through cross-correlation involving the variables (precipitation and temperature) in the same station. The results of the calculations are shown in Table 4. For Mexico City, the highest values of cross-correlation between P and T occur at lag $\tau = 0$ (with global average $c(P, T_{max}) = 0.228 \pm 0.064$ between precipitation and maximum temperature, and $c(P, T_{min}) = 0.096 \pm 0.031$ between precipitation and minimum temperature), meaning that once a rainfall event occurred, the closest-related temperature event occurred on the same day. In contrast, for La Mojana, the highest values occur at lag $\tau = 1$ (with global mean value of $c(P, T_{max}) = 0.256 \pm 0.044$ between precipitation and maximum temperature), i.e., once a precipitation event has occurred, the temperature with which it is most closely related occurred on the last day. This result is reasonable when considering the variability of the magnitude of the events in the different regions, being more stable in La Mojana.

Table 4. Cross-correlation values $c(P, T)$ between precipitation P and temperature T (T_{max} or T_{min} as appropriate) for Mexico City and La Mojana.

Mexico City						La Mojana	
Station	$c(P, T_{max})$	$c(P, T_{min})$	Station	$c(P, T_{max})$	$c(P, T_{min})$	Station	$c(P, T_{max})$
MCS1	0.173	0.096	MCS8	0.245	0.063	LMS1	0.307
MCS2	0.254	0.078	MCS9	0.260	0.059	LMS2	0.265
MCS3	0.279	0.102	MCS10	0.187	0.129	LMS3	0.176
MCS4	0.291	0.070	MCS11	0.280	0.080	LMS4	0.266
MCS5	0.259	0.079	MCS12	0.261	0.136	LMS5	0.214
MCS6	0.039	0.169	MCS13	0.215	0.081	LMS6	0.308
MCS7	0.231	0.115	MCS14	0.211	0.087	LMS7	0.255

3.2.2. Coherence Function

The coherence function shows several bands of high synchronization at different frequencies for Mexico City (See Figure 4a and Figure 4b corresponding to P vs. T_{max} and P vs. T_{min}, respectively), while La Mojana (Figure 4c for P vs. T_{max}) has only one frequency band where the synchronization is high. It is reasonable to attribute this behavior to the seasonality effect for Mexico City, i.e., the coherence values are related to its seasonal condition, giving several bands of synchronization in terms of their frequencies. Indeed, because of its lack of seasonality, La Mojana exhibits only one frequency band, suggesting that using specific frequency bands to analyze climate records will lead to a better characterization of climate records. In general, for Mexico City, the global average coherence between P and T_{max} is 0.061 ± 0.018 (average $\pm$ standard deviation), while between P and T_{min}, it is slightly higher with a mean value of 0.064 ± 0.026. On the other hand, for La Mojana, the average coherence between P and T_{max} has a global mean value of 0.088 ± 0.017. Regardless of the seasonality effect, note that La Mojana exhibits higher global average coherence than Mexico City, meaning more synchronization of the analyzed variables for the former.
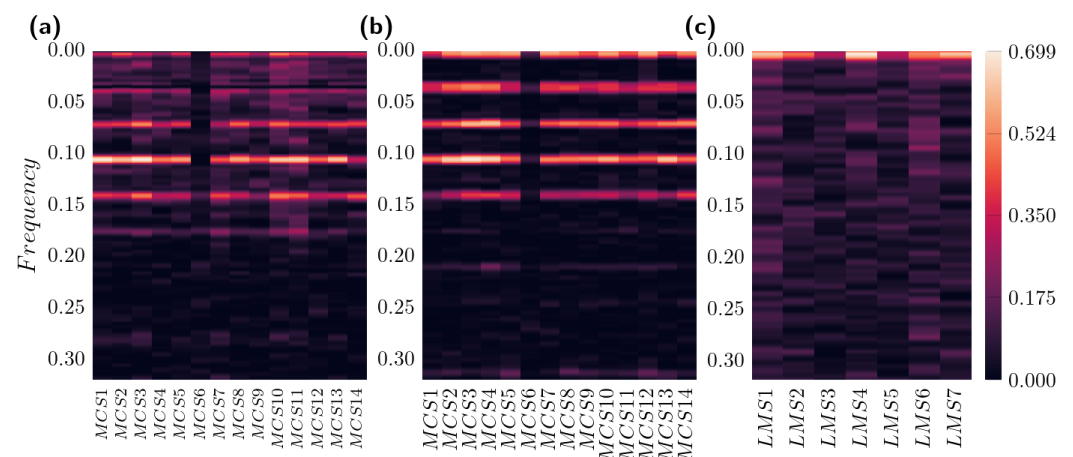
Figure 4. Coherence function heatmap of (**a**) P vs. T_{max}, (**b**) P vs. T_{min} for Mexico City and (**c**) P vs. T_{max} for La Mojana.

3.2.3. Mutual Information

As shown in Table 5, for Mexico City, *MI* has greater values for P and T_{max} than P and T_{min}. The average values are the following: $MI(P, T_{max}) = 1.14 \pm 0.29$ and $MI(P, T_{min}) = 1.08 \pm 0.26$ (clearly $MI(P, T_{max}) > MI(P, T_{min})$). These results indicate that precipitation shares more information with the maximum temperature than with the minimum one. For La Mojana, the mean value is $MI(P, T_{max}) = 1.67 \pm 0.20$, and, in general, *MI* exhibits

higher values compared to those observed in Mexico City, confirming that both variables share more information for this region.

Table 5. Mutual information $MI(P, T)$ for P and T (T_{max} and T_{min}) in Mexico City and La Mojana.

Mexico City						La Mojana	
Station	$MI(P, T_{max})$	$MI(P, T_{min})$	**Station**	$MI(P, T_{max})$	$MI(P, T_{min})$	**Station**	$MI(P, T_{max})$
MCS1	1.65	1.47	MCS8	1.48	1.37	LMS1	1.73
MCS2	1.21	1.13	MCS9	1.40	1.27	LMS2	1.93
MCS3	1.60	1.48	MCS10	1.64	1.47	LMS3	1.45
MCS4	1.20	1.09	MCS11	1.20	1.08	LMS4	1.69
MCS5	1.16	1.09	MCS12	1.18	1.14	LMS5	1.57
MCS6	0.99	0.90	MCS13	2.00	1.83	LMS6	1.44
MCS7	1.36	1.22	MCS14	1.03	0.98	LMS7	1.91

3.2.4. Phase Synchronization Index of Hilbert Transform

The calculations of the γ-index are shown in Table 6 for both regions. For Mexico City data, similar γ-values are observed when they come from either P and T_{max} or P and T_{min}. We find that La Mojana leads to higher vales compared to Mexico City. In general, according to Table 6, values of $\gamma_{P,T}$ are above 0.72 for Mexico City, whereas for La Mojana, the values are above 0.92.

Table 6. Phase synchronization index $\gamma(P, T)$ using Hilbert transform between precipitation P and temperature T (T_{max} or T_{min}) for Mexico City and La Mojana.

Mexico City						La Mojana	
Station	$\gamma(P, T_{max})$	$\gamma(P, T_{min})$	**Station**	$\gamma(P, T_{max})$	$\gamma(P, T_{min})$	**Station**	$\gamma(P, T_{max})$
MCS1	0.739	0.741	MCS8	0.743	0.733	LMS1	0.927
MCS2	0.742	0.733	MCS9	0.740	0.735	LMS2	0.926
MCS3	0.739	0.736	MCS10	0.747	0.736	LMS3	0.925
MCS4	0.744	0.739	MCS11	0.748	0.742	LMS4	0.929
MCS5	0.739	0.736	MCS12	0.745	0.739	LMS5	0.925
MCS6	0.728	0.739	MCS13	0.743	0.738	LMS6	0.926
MCS7	0.745	0.737	MCS14	0.742	0.732	LMS7	0.926

3.2.5. Cross Sample Entropy CSE

As a synchronic measure, CSE values close to zero mean synchrony, while higher values mean asynchrony. Table 7 shows the obtained results for this measure. In addition, to ensure that the information obtained by this metric comes from the behavior of the time series and not from spurious correlations, we also calculate the CSE for the random (shuffled) version of the time series.

The average CSE_E between precipitation and maximum temperature for Mexico City is 1.059 ± 0.276, whereas the average CSE_R for randomized time series is 3.491 ± 0.592. There is a similar occurrence between the precipitation and minimum temperature (for Mexico City), where the average values satisfy $CSE_R > CSE_E$. For La Mojana, the average CSE_E between precipitation and maximum temperature is 0.960 ± 0.404, and CSE_R has a value of 3.409 ± 0.327. In general, the average CSE_E from Mexico City is (about 10%) greater compared with the values obtained from La Mojana, which is in agreement with the results obtained with all previously explored metrics, i.e., a higher synchronization is observed in the latter region.

Table 7. Cross-sample entropy *CSE* (CSE_E for experimental and CSE_R for randomized time series) for *P* and *T* (T_{max} and T_{min} as appropriate) in Mexico City and La Mojana, setting $m = 6$ and $r = 0.20$.

Mexico City										
Station	**(P, T_{max})**		**(P, T_{min})**		**Station**	**(P, T_{max})**		**(P, T_{min})**	
	CSE_E	CSE_R	CSE_E	CSE_R		CSE_E	CSE_R	CSE_E	CSE_R
MCS1	1.385	3.288	0.837	2.010	MCS8	0.894	3.823	0.791	2.093
MCS2	0.657	3.950	0.421	1.901	MCS9	0.791	3.474	0.668	3.051
MCS3	0.797	3.150	0.664	2.802	MCS10	0.824	3.548	1.059	3.298
MCS4	1.744	2.552	0.987	2.792	MCS11	1.062	3.567	1.065	3.164
MCS5	1.089	3.779	0.602	4.562	MCS12	1.048	4.025	1.192	3.535
MCS6	1.170	2.944	1.411	2.315	MCS13	1.169	3.407	1.315	3.703
MCS7	1.058	2.583	1.030	3.075	MCS14	1.136	4.790	0.779	2.849

La Mojana		
Station	**(P, T_{max})**	
	CSE_E	CSE_R
LMS1	0.437	3.675
LMS2	0.966	3.602
LMS3	1.337	3.751
LMS4	1.590	3.564
LMS5	0.435	3.105
LMS6	0.813	3.394
LMS7	1.142	2.772

3.3. Statistical Significance Test for the Synchronization Metrics

To distinguish if the synchronization measures are different between the two studied regions, we test the statistical significance of our results for the coupling measures involving precipitation and maximum temperature using *t*-Student and Mann–Whitney tests, stating as a null hypothesis that, with 95% confidence level, the metrics are the same for both regions. The results are presented in Table 8.

Table 8. List of *p*-values to compare the statistical differences between the synchronization measures from the two regions (Mexico City and La Mojana), for precipitation and maximum temperature at a confidence level of 95%.

Coupling Measure	**p-Value (t-Student)**	**p-Value (Mann–Whitney)**
Cross-Correlation	0.3182	0.2872
Coherence	0.0019	0.0056
Global Phase Synchronization Index	4.62E-27	0.0003
Mutual Information	0.0050	0.0100
Cross-Sample Entropy	3.25E-11	0.0003

Note from Table 8 that, except for cross-correlation, the explored metrics are different between the regions (*p*-value $<<$ 0.05) for both *t*-student and Mann–Whitney tests. The cross-correlation is able to measure relationships between two random variables that follow a linear behavior; however, as they do not show to be different between the two regions, this is most likely due to the nonlinearity of the variables studied, which can be considered a manifestation of the higher complexity that characterizes their joint evolution.

4. Discussion and Conclusions

We have presented a study, based on linear and nonlinear synchronization measures, to identify the level of coupling between daily precipitation and extreme daily temperature records of climate stations from two regions. We find that the degree of coupling is

approximately similar for stations in the same region, while when comparing the two regions analyzed, which have dissimilar climatic characteristics, there is a significant difference (at a confidence level of 95%) in the degree of coupling.

The information presented is consistent and is in agreement with those reported in the literature regarding spatial behavior and complexity [38–42,76–79]. There is evidence that, in a climatic station, precipitation and daily extreme temperatures share information on its dynamics. At first, the results obtained confirm that precipitation data from the two regions exhibit a persistent behavior and temperature records display even more persistent features. When comparing the records from both regions, it is observed that the persistence is greater in the case of La Mojana, indicating that both precipitation and temperature from Mexico City display higher variability that resembles more erratic variations (less memory).

The global information shared between these variables is evidenced by metrics such as those used in this work; however, due to the nonlinear nature of these relationships, it was found that linear metrics such as cross correlation and coherence do not measure interdependence in a robust way, although they provide some characteristics that allow making analysis decisions such as the selection of bands for the detailed study of the time series in the frequency domain as evidenced by coherence. It was also corroborated that metrics such as mutual information quantify the flow of information between the variables studied, being very significant in this case. Our results show different levels of interdependence between precipitation and temperature, demonstrating that these intensities in the associations between the variables depend strongly on the geographic region and local effects that significantly impact the dynamics of these climatic variables. Particularly, our results have indicated that data from Mexico City exhibit a lower synchrony compared to data from La Mojana. This has been verified in the five metrics used to characterize the interdependence between the signals.

The differences in the level of coupling between the regions studied can be explained in the context of greater variability in the case of Mexico City, where seasonality is very important, while in the Mojana area, this component is almost absent. Further studies that include a number of regions with diverse local conditions are needed to better characterize the zones by the levels of coupling achieved and to determine general patterns that will help to better understand these climatic variables.

Future directions for this type of studies could include the identification of possible precursor patterns of extreme values in the variables that could be linked to a greater coupling between the signals or to a lower synchrony, as well as causality, including the use of strategies of topological data analysis to study the synchronization phenomena as used in [80,81]. In summary, the interdependence between temperature and precipitation is of vital importance for a better understanding of climate dynamics, with implications ranging from the environmental impacts already evidenced by climate change to economic and social consequences.

References

1. Schiff, S.J.; So, P.; Chang, T.; Burke, R.E.; Sauer, T. Detecting dynamical interdependence and generalized synchrony through mutual prediction in a neural ensemble. *Phys. Rev. E* **1996**, *54*, 6708–6724. https://doi.org/10.1103/PhysRevE.54.6708.

2. Kreuz, T.; Mormann, F.; Andrzejak, R.G.; Kraskov, A.; Lehnertz, K.; Grassberger, P. Measuring synchronization in coupled model systems: A comparison of different approaches. *Phys. D Nonlinear Phenom.* **2007**, *225*, 29–42. https://doi.org/10.1016/j.physd.2006.09.039.

3. Odenweller, A.; Donner, R.V. Disentangling synchrony from serial dependency in paired-event time series. *Phys. Rev. E* **2020**, *101*, 052213. https://doi.org/10.1103/PhysRevE.101.052213.

4. Kuramoto, Y. Self-entrainment of a population of coupled non-linear oscillators. In *Proceedings of the International Symposium on Mathematical Problems in Theoretical Physics*; Araki, H., Ed.; Springer: Berlin/Heidelberg, Germany, 1975; pp. 420–422. https://doi.org/10.1007/BFb0013365.

5. Rosenblum, M.G.; Pikovsky, A.S.; Kurths, J. Phase Synchronization of Chaotic Oscillators. *Phys. Rev. Lett.* **1996**, *76*, 1804–1807. https://doi.org/10.1103/PhysRevLett.76.1804.

6. Rosenblum, M.; Kurths, J., Analysing Synchronization Phenomena from Bivariate Data by Means of the Hilbert Transform. In *Nonlinear Analysis of Physiological Data*; Springer: Berlin/Heidelberg, Germany, 1998; pp. 91–99. https://doi.org/10.1007/978-3-642-71949-3_6.

7. Rosenblum, M.; Pikovsky, A.; Kurths, J.; Schafer, C.; Tass, P. Chapter 9 Phase synchronization: From theory to data analysis. *Handb. Biol. Phys.* **2001**, *4*, 279–321. https://doi.org/10.1016/S1383-8121(01)80012-9.

8. Rodrigues, F.A.; Peron, T.K.D.; Ji, P.; Kurths, J. The Kuramoto model in complex networks. *Phys. Rep.* **2016**, *610*, 1–98. https://doi.org/10.1016/j.physrep.2015.10.008.

9. Acebrón, J.A.; Bonilla, L.L.; Pérez Vicente, C.J.; Ritort, F.; Spigler, R. The Kuramoto model: A simple paradigm for synchronization phenomena. *Rev. Mod. Phys.* **2005**, *77*, 137–185. https://doi.org/10.1103/RevModPhys.77.137.

10. Pincus, S.M. Approximate entropy as a measure of system complexity. *Proc. Natl. Acad. Sci. USA* **1991**, *88*, 2297–2301. https://doi.org/10.1073/pnas.88.6.2297.

11. Pincus, S.M.; Huang, W.M. Approximate entropy: Statistical properties and applications. *Commun. Stat.-Theory Methods* **1992**, *21*, 3061–3077. https://doi.org/10.1080/03610929208830963.

12. Pincus, S. Approximate entropy (ApEn) as a complexity measure. *Chaos Interdiscip. J. Nonlinear Sci.* **1995**, *5*, 110–117. https://doi.org/10.1063/1.166092.

13. Richman, J.S.; Moorman, J.R. Physiological time-series analysis using approximate entropy and sample entropy. *Am. J. Physiol.-Heart Circ. Physiol.* **2000**, *278*, H2039–H2049. https://doi.org/10.1152/ajpheart.2000.278.6.H2039.

14. Lake, D.E.; Richman, J.S.; Griffin, M.P.; Moorman, J.R. Sample entropy analysis of neonatal heart rate variability. *Am. J. Physiol.-Regul. Integr. Comp. Physiol.* **2002**, *283*, R789–R797. https://doi.org/10.1152/ajpregu.00069.2002.

15. Quian Quiroga, R.; Kraskov, A.; Kreuz, T.; Grassberger, P. Performance of different synchronization measures in real data: A case study on electroencephalographic signals. *Phys. Rev. E* **2002**, *65*, 041903. https://doi.org/10.1103/PhysRevE.65.041903.

16. Costa, M.; Goldberger, A.L.; Peng, C.K. Multiscale entropy analysis of biological signals. *Phys. Rev. E* **2005**, *71*, 021906. https://doi.org/10.1103/PhysRevE.71.021906.

17. Zhang, T.; Yang, Z.; Coote, J.H. Cross-sample entropy statistic as a measure of complexity and regularity of renal sympathetic nerve activity in the rat. *Exp. Physiol.* **2007**, *92*, 659–669. https://doi.org/10.1113/expphysiol.2007.037150.

18. Reyes-Ramírez, I.; Guzmán-Vargas, L. Scaling properties of excursions in heartbeat dynamics. *Europhys. Lett.* **2010**, *89*, 38008. https://doi.org/10.1209/0295-5075/89/38008.

19. Xie, H.B.; Guo, J.Y.; Zheng, Y.P. Fuzzy approximate entropy analysis of chaotic and natural complex systems: Detecting muscle fatigue using electromyography signals. *Ann. Biomed. Eng.* **2010**, *38*, 1483–1496. https://doi.org/10.1007/s10439-010-9933-5.

20. Faust, O.; Bairy, M.G. Nonlinear analysis of physiological signals: A review. *J. Mech. Med. Biol.* **2012**, *12*, 1240015. https://doi.org/10.1142/S0219519412400155.

21. Terrien, J.; Germain, G.; Marque, C.; Karlsson, B. Bivariate piecewise stationary segmentation; improved pre-treatment for synchronization measures used on non-stationary biological signals. *Med. Eng. Phys.* **2013**, *35*, 1188–1196. https://doi.org/10.1016/j.medengphy.2012.12.010.

22. Humeau-Heurtier, A. The Multiscale Entropy Algorithm and Its Variants: A Review. *Entropy* **2015**, *17*, 3110–3123. https://doi.org/10.3390/e17053110.

23. Liang, Z.; Wang, Y.; Sun, X.; Li, D.; Voss, L.J.; Sleigh, J.W.; Hagihira, S.; Li, X. EEG entropy measures in anesthesia. *Front. Comput. Neurosci.* **2015**, *9*, 16. https://doi.org/10.3389/fncom.2015.00016.

24. Aguilar-Velázquez, D.; Guzmán-Vargas, L. Critical synchronization and 1/f noise in inhibitory/excitatory rich-club neural networks. *Sci. Rep.* **2019**, *9*, 1–13. https://doi.org/10.1038/s41598-018-37920-w.

25. Delgado-Bonal, A.; Marshak, A. Approximate Entropy and Sample Entropy: A Comprehensive Tutorial. *Entropy* **2019**, *21*, 541. https://doi.org/10.3390/e21060541.

26. Jamin, A.; Duval, G.; Annweiler, C.; Abraham, P.; Humeau-Heurtier, A. Study of the influence of Age: Use of Sample Entropy and CEEMDAN on Navigation Data Acquired from a Bike Simulator. In Proceedings of the 2020 Tenth International Conference on Image Processing Theory, Tools and Applications (IPTA), Paris, France, 9–12 November 2020; pp. 1–6. https://doi.org/10.1109/IPTA50016.2020.9286648.

27. Kleinbub, J.R.; Talia, A.; Palmieri, A. Physiological synchronization in the clinical process: A research primer. *J. Couns. Psychol.* **2020**, *67*, 420. https://doi.org/10.1037/cou0000383.

28. Pincus, S. Approximate Entropy as an Irregularity Measure for Financial Data. *Econom. Rev.* **2008**, *27*, 329–362. https://doi.org/10.1080/07474930801959750.

29. Liu, L.Z.; Qian, X.Y.; Lu, H.Y. Cross-sample entropy of foreign exchange time series. *Phys. A Stat. Mech. Its Appl.* **2010**, *389*, 4785–4792. https://doi.org/10.1016/j.physa.2010.06.013.

30. Shi, W.; Shang, P. Cross-sample entropy statistic as a measure of synchronism and cross-correlation of stock markets. *Nonlinear Dyn.* **2013**, *71*, 539–554. https://doi.org/10.1007/s11071-012-0680-z.

31. David E Allen, M.M.; Singh, A.K. An entropy-based analysis of the relationship between the DOW JONES Index and the TRNA Sentiment series. *Appl. Econ.* **2017**, *49*, 677–692. https://doi.org/10.1080/00036846.2016.1203067.

32. Hernández-Pérez, R.; Guzmán-Vargas, L.; Ramírez-Rojas, A.; Angulo-Brown, F. Pattern synchrony in electrical signals related to earthquake activity. *Phys. A Stat. Mech. Its Appl.* **2010**, *389*, 1239–1252. https://doi.org/10.1016/j.physa.2009.11.036.

33. Balasis, G.; Donner, R.V.; Potirakis, S.M.; Runge, J.; Papadimitriou, C.; Daglis, I.A.; Eftaxias, K.; Kurths, J. Statistical Mechanics and Information-Theoretic Perspectives on Complexity in the Earth System. *Entropy* **2013**, *15*, 4844–4888. https://doi.org/10.3390/e15114844.

34. Balasis, G.; Balikhin, M.A.; Chapman, S.C.; Consolini, G.; Daglis, I.A.; Donner, R.V.; Kurths, J.; Paluš, M.; Runge, J.; Tsurutani, B.T.; et al. Complex Systems Methods Characterizing Nonlinear Processes in the Near-Earth Electromagnetic Environment: Recent Advances and Open Challenges. *Space Sci. Rev.* **2023**, *219*, 82. https://doi.org/10.1007/s11214-023-00979-7.

35. Reyes-Ramírez, I.; Martínez-Boggio, S.D.; Curto-Risso, P.L.; Medina, A.; Calvo Hernández, A.; Guzmán-Vargas, L. Symbolic Analysis of the Cycle-to-Cycle Variability of a Gasoline–Hydrogen Fueled Spark Engine Model. *Energies* **2018**, *11*, 968. https://doi.org/10.3390/en11040968.

36. Dijkstra, H.A. *Nonlinear Climate Dynamics*; Cambridge University Press: Cambridge, UK, 2013. https://doi.org/10.1017/CBO9781139034135.

37. Varotsos, C.; Sarlis, N.V.; Mazei, Y.; Saldaev, D.; Efstathiou, M. A Composite Tool for Forecasting El Niño: The Case of the 2023–2024 Event. *Forecasting* **2024**, *6*, 187–203. https://doi.org/10.3390/forecast6010011.

38. Duane, G.S. Synchronized chaos in extended systems and meteorological teleconnections. *Phys. Rev. E* **1997**, *56*, 6475–6493. https://doi.org/10.1103/PhysRevE.56.6475.

39. Berg, P.; Haerter, J.O.; Thejll, P.; Piani, C.; Hagemann, S.; Christensen, J.H. Seasonal characteristics of the relationship between daily precipitation intensity and surface temperature. *J. Geophys. Res. Atmos.* **2009**, *114*, 1–9. https://doi.org/10.1029/2009JD012008.

40. Donges, J.F.; Zou, Y.; Marwan, N.; Kurths, J. Complex networks in climate dynamics: Comparing linear and nonlinear network construction methods. *Eur. Phys. J. Spec. Top.* **2009**, *174*, 157–179. https://doi.org/10.1140/epjst/e2009-01098-2.

41. Feliks, Y.; Ghil, M.; Robertson, A.W. Oscillatory Climate Modes in the Eastern Mediterranean and Their Synchronization with the North Atlantic Oscillation. *J. Clim.* **2010**, *23*, 4060–4079. https://doi.org/10.1175/2010JCLI3181.1.

42. Gennaretti, F.; Sangelantoni, L.; Grenier, P. Toward daily climate scenarios for Canadian Arctic coastal zones with more realistic temperature-precipitation interdependence. *J. Geophys. Res. Atmos.* **2015**, *120*, 11862–11877. https://doi.org/10.1002/2015JD023890.

43. Jajcay, N.; Kravtsov, S.; Sugihara, G.; Tsonis, A.A.; Paluš, M. Synchronization and causality across time scales in El Niño Southern Oscillation. *Npj Clim. Atmos. Sci.* **2018**, *1*, 33.

44. Thota, S.; Nassar, A.; Filali Boubrahimi, S.; Hamdi, S.M.; Hosseinzadeh, P. Enhancing Monthly Streamflow Prediction Using Meteorological Factors and Machine Learning Models in the Upper Colorado River Basin. *Hydrology* **2024**, *11*, 66. https://doi.org/10.3390/hydrology11050066.

45. Jingjie Yu, Guobin Fu, W.C.; Cowan, T. Impacts of precipitation and temperature changes on annual streamflow in the Murray–Darling Basin. *Water Int.* **2010**, *35*, 313–323, https://doi.org/10.1080/02508060.2010.484907.

46. Rahmani, F.; Fattahi, M.H. A multifractal cross-correlation investigation into sensitivity and dependence of meteorological and hydrological droughts on precipitation and temperature. *Nat. Hazards* **2021**, *109*, 2197–2219.

47. Aquino-Martínez, L.P.; Quintanar, A.I.; Ochoa-Moya, C.A.; López-Espinoza, E.D.; Adams, D.K.; Jazcilevich-Diamant, A. Urban-Induced Changes on Local Circulation in Complex Terrain: Central Mexico Basin. *Atmosphere* **2021**, *12*, 904. https://doi.org/10.3390/atmos12070904.

48. María, A.D. La Mojana: Riqueza natural y potencial económico. Technical report, DTSER-48, Banco de la República, sep 2004, Bogotá D.C., Colombia, 1–73. https://www.banrep.gov.co/es/mojana-riqueza-natural-y-potencial-economico, (last accessed date: 8 May 2024)

49. Zabaleta, A.; Mercado, T.; Marrugo, J.L.; Feria, J. Curve Number (CN) as Pressure Indicator of the Hydrological Condition under Global Warming Scenarios at a Local Scale in La Mojana Region, Colombia. *Indian J. Sci. Technol.* **2018**, *11*, 1–12. https://doi.org/10.17485/ijst/2018/v11i29/129276.

50. Tukey, J.W. *Exploratory Data Analysis*; Addison-Wesley Series in Behavioral Science: Quantitative Methods 7616; Addison Wesley: Boston, MA, USA, 1977.

51. Velleman, P.F.; Hoaglin, D.C. *Applications, Basics, and Computing of Exploratory Data Analysis*; Duxbury Press: New York, NY, USA, 1981.

52. Tukey, J., Exploratory Data Analysis. In *The Concise Encyclopedia of Statistics*; Springer: New York, NY, USA, 2008; pp. 192–194. https://doi.org/10.1007/978-0-387-32833-1_136.

53. Mukhiya, S.K.; Ahmed, U. *Hands-On Exploratory Data Analysis with Python: Perform EDA Techniques to Understand, Summarize, and Investigate Your Data*; Packt Publishing Ltd.: Birmingham, UK, 2020.

54. Hurst, H.E. The problem of long-term storage in reservoirs. *Int. Assoc. Sci. Hydrology. Bull.* **1956**, *1*, 13–27. https://doi.org/10.1080/02626665609493644.

55. Higuchi, T. Approach to an irregular time series on the basis of the fractal theory. *Phys. D Nonlinear Phenom.* **1988**, *31*, 277–283. https://doi.org/10.1016/0167-2789(88)90081-4.

56. Rangarajan, G.; Ding, M. Integrated approach to the assessment of long range correlation in time series data. *Phys. Rev. E* **2000**, *61*, 4991–5001. https://doi.org/10.1103/PhysRevE.61.4991.

57. Guzmán-Vargas, L.; Angulo-Brown, F. Simple model of the aging effect in heart interbeat time series. *Phys. Rev. E* **2003**, *67*, 052901. https://doi.org/10.1103/PhysRevE.67.052901.

58. Bunde, A.; Kropp, J.; Schellnhuber, H. *The Science of Disasters: Climate Disruptions, Heart Attacks, and Market Crashes*; Springer Science & Business Media: Berlin, Germany, 2012.

59. Derrick, T.; Thomas, J.M., The cross-correlation function. In *Time Series Analysis*; Iowa State University: Ames, IA, USA, 2004; Chapter 7.

60. Kohn, A.F., Autocorrelation and Cross-Correlation Methods. In *Wiley Encyclopedia of Biomedical Engineering*; John Wiley & Sons, Ltd.: Hoboken, NJ, USA, 2006; Chapter 4, pp. 260–283. https://doi.org/10.1002/9780471740360.ebs0094.

61. Bracewell, R.N. *The Fourier Transform and Its Applications*, 3rd ed.; Electrical Engineering Series; McGraw-Hill: New York, NY, USA, 1966. https://doi.org/10.2307/2314845.

62. Bendat, J.S.; Piersol, A.G. *Random Data: Analysis and Measurement Procedures*; Wiley Series in Probability and Statistics; John Wiley & Sons: Hoboken, NJ, USA, 2011. https://doi.org/10.1002/9781118032428.

63. Paluš, M.; Komárek, V.; Hrnčíř, Z.c.v.; Štěrbová, K. Synchronization as adjustment of information rates: Detection from bivariate time series. *Phys. Rev. E* **2001**, *63*, 046211. https://doi.org/10.1103/PhysRevE.63.046211.

64. Vadlamudi, C.V.; Vadlamudi, S.P.D. Chapter 4 - Mathematical Essentials. In *Computational Analysis and Understanding of Natural Languages: Principles, Methods and Applications*; Gudivada, V.N., Rao, C., Eds.; Handbook of Statistics; Elsevier: Amsterdam, The Netherlands, 2018; Volume 38, pp. 53–73. https://doi.org/10.1016/bs.host.2018.07.008.

65. Wibral, M.; Vicente, R.; Lizier, J.T. *Directed Information Measures in Neuroscience*; Springer: Berlin/Heidelberg, Germany, 2014; Volume 724. https://doi.org/10.1007/978-3-642-54474-3.

66. Rice, J.A.; Rice, J.A. *Mathematical Statistics and Data Analysis*; Thomson/Brooks/Cole: Belmont, CA, USA, 2007; Volume 371.

67. Mann, H.B.; Whitney, D.R. On a Test of Whether one of Two Random Variables is Stochastically Larger than the Other. *Ann. Math. Stat.* **1947**, *18*, 50 – 60. https://doi.org/10.1214/aoms/1177730491.

68. White, L.; Boashash, B. Cross spectral analysis of nonstationary processes. *IEEE Trans. Inf. Theory* **1990**, *36*, 830–835. https://doi.org/10.1109/18.53742.

69. Koscielny-Bunde, E.; Bunde, A.; Havlin, S.; Roman, H.E.; Goldreich, Y.; Schellnhuber, H.J. Indication of a Universal Persistence Law Governing Atmospheric Variability. *Phys. Rev. Lett.* **1998**, *81*, 729–732. https://doi.org/10.1103/PhysRevLett.81.729.

70. Eichner, J.F.; Koscielny-Bunde, E.; Bunde, A.; Havlin, S.; Schellnhuber, H.J. Power-law persistence and trends in the atmosphere: A detailed study of long temperature records. *Phys. Rev. E* **2003**, *68*, 046133. https://doi.org/10.1103/PhysRevE.68.046133.

71. Fraedrich, K.; Blender, R. Scaling of Atmosphere and Ocean Temperature Correlations in Observations and Climate Models. *Phys. Rev. Lett.* **2003**, *90*, 108501. https://doi.org/10.1103/PhysRevLett.90.108501.

72. Miranda, J.G.V.; Andrade, R.F.S.; Da Silva, A.; Ferreira, C.; González, A.P.; Carrera López, J. Temporal and spatial persistence in rainfall records from Northeast Brazil and Galicia (Spain). *Theor. Appl. Climatol.* **2004**, *77*, 113–121. https://doi.org/10.1007/s00704-003-0013-8.

73. Tsekov, M. Long-term correlations in weather records from a local place in south Bulgaria. *Comptes Rendus De l'Academie Bulg. Des Sci.* **2004**, *57*, 6–61.

74. Kantelhardt, J.W.; Koscielny-Bunde, E.; Rybski, D.; Braun, P.; Bunde, A.; Havlin, S. Long-term persistence and multifractality of precipitation and river runoff records. *J. Geophys. Res. Atmos.* **2006**, *111*. https://doi.org/10.1029/2005JD005881.

75. Yang, L.; Fu, Z. Process-dependent persistence in precipitation records. *Phys. A Stat. Mech. Its Appl.* **2019**, *527*, 121459. https://doi.org/10.1016/j.physa.2019.121459.

76. Choobeh, S.; Abghari, H.; Erfanian, M. Spatial and temporal variability of precipitation based on marginal and apportionment entropy disorder indices in Iran. *Theor. Appl. Climatol.* **2024**, *155*, 2589–2603. https://doi.org/10.1007/s00704-023-04748-y.

77. Abbasnezhadi, K.; Rousseau, A.N.; Wruth, A.M.; Zahmatkesh, Z. Synchronized generation of high-resolution gridded precipitation and temperature fields. *J. Hydrol.* **2019**, *573*, 631–647. https://doi.org/10.1016/j.jhydrol.2019.03.096.

78. Rybski, D.; Havlin, S.; Bunde, A. Phase synchronization in temperature and precipitation records. *Phys. A Stat. Mech. Its Appl.* **2003**, *320*, 601–610. https://doi.org/10.1016/S0378-4371(02)01509-1.

79. Ogunjo, S.; Fuwape, I.; Oluyamo, S.; Rabiu, B. Spatial Dynamical Complexity of Precipitation and Temperature Extremes over Africa and South America. *Asia-Pac. J. Atmos. Sci.* **2024**, *60*, 15–28. https://doi.org/10.1007/s13143-019-00131-y.

80. Zabaleta-Ortega, A.; Masoller, C.; Guzmán-Vargas, L. Topological data analysis of the synchronization of a network of Rössler chaotic electronic oscillators. *Chaos Interdiscip. J. Nonlinear Sci.* **2023**, *33*, 113110. https://doi.org/10.1063/5.0167523.

81. Guzman-Vargas, L.; Zabaleta-Ortega, A.; Guzman-Saenz, A. Simplicial complex entropy for time series analysis. *Sci. Rep.* **2023**, *13*. https://doi.org/10.1038/s41598-023-49958-6.